Fuel 189 (2017) 8–14

Contents lists available at ScienceDirect

Fuel

journal homepage: www.elsevier.com/locate/fuel

Full Length Article

Flame–wall interactions of lean premixed flames under elevated, rising pressure conditions

Basmil Yenerdag [a,*], Yuki Minamoto [a], Kozo Aoki [a], Masayasu Shimura [a], Yuzuru Nada [b], Mamoru Tanahashi [a]

[a] Department of Mechanical Engineering, Tokyo Institute of Technology, 2-12-1 Ookayama, Meguro-ku, Tokyo 152-8550, Japan
[b] Department of Energy System, Tokushima University, 2-1 Minami-josanjima, Tokushima 770-8506, Japan

HIGHLIGHTS

- Flame–wall interactions of hydrocarbon flames are studied using 1D DNS.
- Flame–wall interaction time can be scaled by flame time at fixed wall temperature.
- Effects of pressure increase on flame–wall interaction time are insignificant.
- Effects of LTHR in *n*-heptane flames on wall heat flux are insignificant.

ARTICLE INFO

Article history:
Received 31 May 2016
Received in revised form 17 October 2016
Accepted 19 October 2016
Available online 24 October 2016

Keywords:
Laminar premixed flames
Direct numerical simulation
Pressure rising process
Wall heat flux
Flame–wall interactions

ABSTRACT

Direct numerical simulation (DNS) of laminar lean methane–air and *n*-heptane–air premixed flames with high exhaust gas recirculation (EGR) ratios propagating towards inert walls in a head-on quenching configuration is conducted to investigate flame–wall interactions at relatively high initial pressure conditions. This study considers the flame propagation under isochoric process after ignition while the piston is at top dead center (TDC). The effects of EGR ratio, equivalence ratio, initial pressure and wall temperature on heat loss and quenching distance are investigated. The results showed that change of EGR ratio in fuel mixture significantly affects the maximum wall heat flux and the heat flux induced by the burned gas temperature. The normalized flame–wall interaction time is not influenced over a range of EGR ratios, equivalence ratios and initial chamber pressures for methane–air and *n*-heptane–air flames at fixed wall temperature conditions. The dimensional flame–wall interaction time is almost constant when the chamber pressure is doubled. The influence of low temperature oxidation in *n*-heptane flames on wall heat flux induced by temperature differences between the preheated fuel mixture and the wall is found to be insignificant. Moreover, both thermal conductivity near the wall and quenching distance are sensitive to the wall temperature, and have a substantial influence on the wall heat flux.

1. Introduction

As emission regulations become more stringent, achieving both higher thermal efficiencies and reduced pollutant emissions is key to designing combustion devices. Recently, lean-boosted combustion with a high exhaust gas recirculation (EGR) level has been of particular interest for automotive engines, because both combustion efficiency and pollutant reduction are improved. The presence of diluted reactants further decreases the end-gas temperature and improves knock resistance [1,2]. In addition, it was shown that the effective octane number can be increased by increasing the EGR ratio of the fuel mixtures [2]. However, heat loss characteristics are likely to be modified by such thermo-chemical conditions. Therefore, to achieve higher thermal efficiency by further reducing wall heat loss, it is important to understand heat transfer characteristics through the wall as well as the effects of relevant parameters such as EGR ratio γ, equivalence ratio ϕ, and wall temperature T_{wall} on these characteristics.

With improvements in computational technology, direct numerical simulation (DNS) has become an important tool for investigating flame–wall interactions. Important quantities of flame–wall interaction phenomenon such as maximum wall heat flux and quenching distance have been extensively studied in previous numerical studies [3–8]. Interactions of laminar hydrogen premixed flames with walls have been studied in a head-on quenching configuration using a one-dimensional DNS with detailed chemistry in Refs. [3,4]. Dabireau et al. [3] have shown

* Corresponding author.
E-mail address: ybasmil@navier.mes.titech.ac.jp (B. Yenerdag).

http://dx.doi.org/10.1016/j.fuel.2016.10.096
0016-2361/

Nomenclature

γ	EGR ratio
ϕ	equivalence ratio
T_{wall}	wall temperature
T	temperature
T_u	unburned temperature
T_b	burned temperature
T_{wall}	wall temperature
T_{pre}	preheated temperature
T_{ini}	initial temperature distribution
T_{max}	maximum temperature
$T_{ad,0}$	adiabatic flame temperature
P_{ini}	initial chamber pressure
r_c	radius of the ignition kernel
σ_T	the distance from center to the position at which the temperature gradient is maximum
Φ_q	wall heat flux
Φ_n	normalized maximum wall heat flux
Φ_f	laminar flame power
$\delta_{th,0}$	thermal flame thickness at initial pressure conditions
$S_{L,0}$	laminar burning velocity at initial pressure conditions
ϕ	equivalence ratio
ρ	density
$\boldsymbol{u}$	fluid velocity vector
λ	thermal conductivity of the gaseous mixture
N_s	number of chemical species
Y_i	mass fraction for species i
$\boldsymbol{V}_i$	diffusion velocity for chemical species i
R_i	characteristic gas constant for chemical species i
h_i	enthalpy for chemical species i
w_i	reaction rate for chemical species i
$c_{v,i}$	heat capacity at constant volume for chemical species i
$c_{p,i}$	heat capacity at constant pressure for chemical species i
$\bar{c_v}$	mixture averaged specific heat capacity at constant volume
$\boldsymbol{P}$	stress tensor
p	pressure
μ	dynamic viscosity
$\tau_{F,0}$	flame time at initial pressure conditions
τ_{fw}	flame–wall interaction time

that at atmospheric pressure with inert boundary conditions, premixed flames generate high heat release rate near the wall than it does away from the wall. Owston et al. [4] investigated the effects of equivalence ratio and pressure on wall heat flux Φ_q, and the results show a significant increase in maximum Φ_q when the pressure is doubled. Owston et al. [5] have also investigated laminar *n*-heptane–air flames at different wall temperatures under constant pressure conditions. They have found a significant increase in the maximum Φ_q with increasing wall temperature from 300 to 1200 K in stoichiometric flames. A similar trend in maximum wall heat flux has also been reported using DNS of laminar stoichiometric methane, propane [6,7] and iso-octane [8] premixed flames with wall temperature ranging from 300 to 600 K. Overall trends of quenching distance and the maximum Φ_q are similar in experimental studies [9,10]. A more detailed discussion of flame–wall interactions on DNS and experimental studies can be found in Ref. [11]. The aforementioned DNS studies on flame–wall interaction phenomenon consider constant pressure conditions. Whereas, in a constant volume vessel such as IC engines, the mean pressure increases during combustion which significantly influences wall heat transfer characteristics via temporal evolution of thermo-chemical properties. One consequence is that flame thickness rapidly decreases with increasing pressure, leading to a decreased quenching distance near the wall. This results in an increased maximum wall heat flux [12]. Therefore, the mechanism influencing overall wall heat flux is based on a complex balance of varying flame properties due to environmental changes in the vessel as combustion proceeds. This mechanism needs to be understood to lower the heat loss for high-efficiency engines. In this study, due to the enormous computational resources required by DNS, a one-dimensional configuration similar to the previous studies [3–8] is employed. Moreover, the compromise made in the numerical configuration is accommodated by employing a more complex chemistry, an isochoric process and relatively high pressure conditions. Thus, the present results add new insight to our knowledge of flame–wall interaction phenomena. This study also serves as a preliminary DNS for the future three-dimensional DNS configuration which is similar to our previous DNS studies [12,13].

In this study, a series of one-dimensional DNS of lean methane–air and *n*-heptane–air premixed flames with different EGR ratios propagating towards inert walls in a head-on quenching configuration is conducted in a constant volume vessel under elevated, rising pressure conditions to investigate the effects of EGR ratio, equivalence ratio, initial pressure and wall temperature on wall heat flux and quenching distance. This paper is organized as follows: The details of the DNS database is explained in Section 2, the results are discussed in Section 3 and the conclusions are summarized in the final section.

2. Direct numerical simulation

The DNS code developed in our previous study [14] is employed. The fully-compressible governing equations for conservation of mass, momentum, energy and chemical species mass fractions, respectively can be written as:

$$\frac{\partial \rho}{\partial t} + \nabla \cdot (\rho \boldsymbol{u}) = 0, \tag{1}$$

$$\frac{\partial \rho \boldsymbol{u}}{\partial t} + (\nabla \rho \boldsymbol{u}\boldsymbol{u}) = -\nabla \cdot \boldsymbol{P}, \tag{2}$$

$$\begin{aligned}\frac{\partial \rho T}{\partial t} + \nabla \cdot (\rho \boldsymbol{u} T) = \frac{1}{\bar{c}_v}\nabla \cdot (\lambda \nabla T) - \frac{1}{\bar{c}_v}\sum_{i=1}^{N_s}\left(\rho Y_i \boldsymbol{V}_i c_{p,i} \nabla T\right) \\ - \frac{T}{\bar{c}_v}\sum_{i=1}^{N_s}[R_i \nabla \cdot (\rho Y_i \boldsymbol{V}_i)] - \frac{1}{\bar{c}_v}\boldsymbol{P} \\ : (\nabla \boldsymbol{u}) - \frac{1}{\bar{c}_v}\sum_{i=1}^{N_s}(h_i w_i) + \frac{T}{\bar{c}_v}\sum_{i=1}^{N_s}(R_i w_i),\end{aligned} \tag{3}$$

$$\frac{\partial Y_i}{\partial t} + \boldsymbol{u} \cdot \nabla Y_i = -\frac{1}{\rho}\nabla \cdot (\rho Y_i \boldsymbol{V}_i) + \frac{w_i}{\rho}. \tag{4}$$

where $\rho, \boldsymbol{u}, T, \lambda$ and N_s denote density, fluid velocity vector, temperature, thermal conductivity and the number of chemical species, respectively. $Y_i, \boldsymbol{V}_i, R_i, h_i, w_i, c_{v,i}$ and $c_{p,i}$ denote, respectively, mass fraction, diffusion velocity, characteristic gas constant, enthalpy, reaction rate, specific heat capacities at constant volume and pressure for chemical species i. The stress tensor, $\boldsymbol{P}$ is given by

$$\boldsymbol{P} = \left[p + \frac{2}{3}\mu(\nabla \cdot \boldsymbol{u})\right]\boldsymbol{I} - \mu\left[(\nabla \boldsymbol{u}) + (\nabla \boldsymbol{u})^T\right], \quad (5)$$

where p, μ and $\boldsymbol{I}$ denote pressure, dynamic viscosity and the unit tensor, respectively. The mixture averaged specific heat capacity at constant volume, $\bar{c_v}$ is given by

$$\bar{c_v} = \sum_{i=1}^{N_s} c_{v,i} Y_i \quad (6)$$

The Soret effect, the Dufour effect, pressure gradient diffusion, bulk viscosity and radiative heat transfer are assumed to be negligible. The GRI-Mech 3.0 kinetic mechanism [15], which includes 53 reactive species and 325 elementary reactions, is used to describe methane–air combustion chemistry. For *n*-heptane–air premixed flames, a reduced kinetic mechanism, which includes 37 reactive species and 61 elementary reactions is used [16]. Temperature dependence of the viscosity, the thermal conductivity and the diffusion coefficients are taken into account by linking the CHEMKIN-II packages [17,18]. The governing equations are discretized using a fourth-order central finite difference scheme, and advanced in time by using the third order Runge-Kutta method with $\Delta t = 1$ ns. The fourth order compact finite difference filter [19] is used to eliminate unphysical oscillations with higher spatial frequencies than the spatial resolution. Only the reaction source terms are advanced by the implicit method [20]. For the boundary condition, isothermal and no-slip conditions expressed in the form of the Navier-Stokes characteristic boundary condition (NSCBC) [22,21] are imposed on both of the walls and the wall surfaces are assumed to be chemically inert. The initial distribution of species mass fraction is uniform.

The schematic of the computational domain representing the constant volume vessel in the present study is shown in Fig. 1a. Fig. 1b shows the initial temperature distribution (T_{ini}) in the domain. The computational domain has a closed configuration with walls at both ends and has a size of $L_x = 5.0$ mm, which is discretized with uniform mesh, ensuring at least 80 grid points within the laminar flame thickness at the initial pressure to resolve the flame–wall interactions. This domain length represents the state when the piston head is at the top dead center (TDC) at the end of the compression stroke. Although this length is smaller than that in practical applications, the present domain length is chosen to allow flames to develop before impinging on the wall. T_{ini} is given as a Gaussian distribution and written as follows:

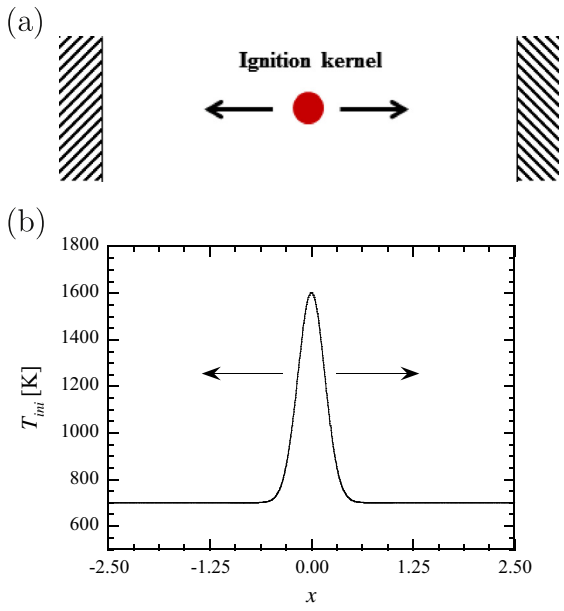

Fig. 1. Schematic of the computational domain (a) and initial temperature distribution in the domain (b). Wall boundary at $x = -2.5$ and 2.5 mm. Arrows indicate the direction of flame propagation after ignition.

$$T_{ini} = T_{pre} + (T_{max} - T_{pre}) \exp\left(-\frac{r^2}{2\sigma_T^2}\right), \quad (7)$$

$$\sigma_T = r_c/3. \quad (8)$$

Here, T_{max}, T_{pre}, r_c, r and σ_T denote the maximum temperature of the ignition kernel, preheat temperature, radius of the ignition kernel, distance from center and the distance from center to position at which the temperature gradient is maximum, respectively.

Table 1 shows the relevant parameters of methane and *n*-heptane flames. γ indicates the EGR ratio. $S_{L,0}, \delta_{th,0}$ and $T_{ad,0}$ denote the laminar burning velocity, the laminar flame thickness based on the maximum temperature gradient, and the adiabatic flame temperature for initial flames, respectively. The subscript 0 indicates the quantity obtained from the laminar flame under constant initial pressure P_{ini} and T_{pre} conditions. In this study, $T_{ini}, T_{max}, T_{pre}$ and r_c are the same for all cases. T_{max} is 1600 K, T_{pre} is 700 K and r_c is taken to be 0.5 mm. The present study simulates the phenomena at which the flame propagates under isochoric process after ignition while the piston is at TDC. After the mixture is ignited at the center of the domain, the flame propagates towards both ends. As the flame propagates, the pressure in the domain increases and the effects of time-varying thermo-chemical properties can be addressed using the present DNS configuration. Since the initial preheated temperature is set to 700 K, the mean pressure (P_{mean}) is expected to increase by a factor of 2.4–2.7 for the present lean hydrocarbon flames. Both methane–air and *n*-heptane–air mixtures are diluted with EGR consisting of O_2, N_2, H_2O and CO_2. The mole fraction of H_2O in EGR is twice that of CO_2 in methane flames and 0.875 times that in *n*-heptane flames. The effects of EGR ratio, equivalence ratio, initial pressure and wall temperature on wall heat flux and quenching distance are discussed.

3. Results and discussions

3.1. Influence of EGR ratio, equivalence ratio and initial pressure

Fig. 2 shows the temporal developments of the mean pressure of the domain as well as the maximum heat flux of methane–air flames for an equivalence ratio of 0.5 at different EGR ratios. Here, mean pressure is defined as pressure averaged in the whole domain. Wall heat flux is defined as the product of the thermal conductivity of the gas mixture and the temperature gradient on the wall, written as follows:

$$\Phi_q = -\lambda \nabla T|_{wall} \quad (9)$$

The wall temperature is fixed at 450 K. The time is normalized using the corresponding characteristic flame time ($\tau_{F,0} = \delta_{th,0}/S_{L,0}$). Therefore $\tau_{F,0}$ is different for each case, and can be calculated from Table 1. For this reason, the flame with the fastest laminar burning velocity (case M10W045) reaches the wall first, but has the largest non-dimensional time duration when it impinges on the wall. Note that the heat flux induced by temperature differences between the preheated fuel mixture and the wall in the early period ($t/\tau_{F,0} < 1$) is high due to the initial developments of a temperature profile near the wall (i.e., the thermal boundary layer development in the 2D and 3D fields.). The heat flux stabilizes after approximately $1\tau_{F,0}$ and has values around 0.1 MW/m^2 for all 3 cases. When the flame impinges on the wall, the wall heat flux at the attached point increases drastically. The maximum Φ_q decreases by 37% when the EGR ratio increase is

Table 1
Numerical parameters for DNS of methane–air and *n*-heptane–air premixed flames.

Methane & *n*-heptane	ϕ	γ (%)	$S_{L,0}$ (m/s)	$\delta_{th,0}$ (mm)	T_{wall} (K)	P_{ini} (atm)	$T_{ad,0}$ (K)
M10W045	0.5	10	0.137	0.208	450	10	1743
M15W045	0.5	15	0.119	0.236	450	10	1713
M20W045	0.5	20	0.102	0.270	450	10	1680
M20W045E	0.6	20	0.166	0.175	450	10	1816
M20W070	0.5	20	0.102	0.270	700	10	1680
M20W090	0.5	20	0.102	0.270	900	10	1680
M20W110	0.5	20	0.102	0.270	1100	10	1680
M20W045P	0.5	20	0.075	0.188	450	20	1680
H20W045	0.5	20	0.156	0.188	450	10	1711
H20W070	0.5	20	0.156	0.188	700	10	1711
H20W090	0.5	20	0.156	0.188	900	10	1711

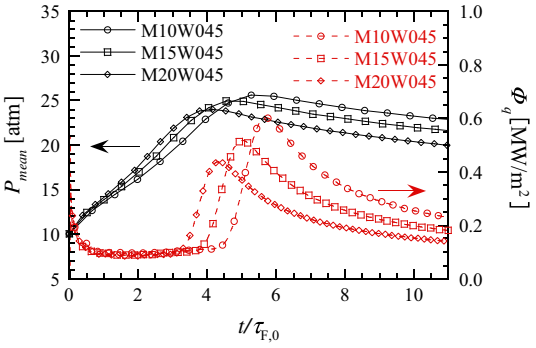

Fig. 2. Temporal developments of mean pressure and wall heat flux of methane flames with different EGR ratio.

10% (M10W045 and M20W045). This is because the flame is thicker at higher EGR ratios. The wall heat flux induced by the burned gas is also reduced since the flame temperature is lower for higher EGR ratios.

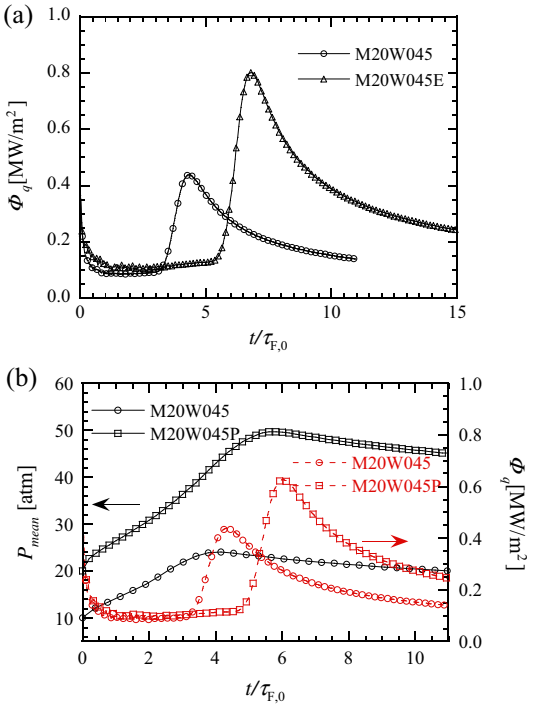

Fig. 3. Temporal developments of wall heat flux of methane flames at different equivalence ratio (a) and at different initial pressure conditions with mean pressure (b).

Fig. 3a shows the temporal developments of wall heat flux for flames with different equivalence ratios. The EGR ratio (γ), initial pressure and wall temperature are kept constant at 20%, 10 atm and 450 K, respectively. It was found that changing the equivalence ratio has a higher impact on the maximum wall heat flux than changing the EGR ratio. The maximum Φ_q is 83% higher for the increased ϕ case, ($\phi = 0.6$, M20W045E), because a thinner flame can reach the wall closer thereby increasing the temperature gradient on the wall. Moreover, the heat flux induced by the burned gas temperature is also higher than that in M20W045 ($\phi = 0.5$) since the flame temperature is higher. Although the time span of the maximum Φ_q acting on the wall is much shorter than that of the wall heat flux induced by burned gas temperature, it was shown that the wall heat flux induced by flame impingement (maximum wall heat flux) contributes substantially to the total heat loss during combustion [13].

The initial pressure is doubled to investigate pressure effects on flame–wall interactions. Fig. 3b shows the temporal developments of mean pressure and maximum heat flux for different initial pressure cases, P_{ini} = 10 atm (M20W045) and P_{ini} = 20 atm (M20W045P). The maximum P_{mean} reaches up to 50 atm when the flame impingement occurs in M20W045P. Since the burning speed is slower in M20W045P, a longer time is required for the flame to reach the wall. However, the flame–wall interaction time τ_{fw}, which can be defined as the time required for Φ_q to reach its maximum from its half value [9], does not seem to be affected when the pressure is doubled. This result is consistent with an experimental study for stoichiometric methane flames under constant pressure conditions (0.5–17 atm) by Sotton et al. [23]. Here, τ_{fw} is 1.93 ms and 1.91 ms for P_{ini} = 10 atm (M20W045) and P_{ini} = 20 atm (M20W045P), respectively. In addition, regardless of any conditions reported in this study – different EGR ratios, equivalence ratios and initial pressures – the normalized τ_{fw} are similar when normalized by $\tau_{F,0}$, and they are in the range of 0.73–0.76$\tau_{F,0}$. The maximum Φ_q of M20W045P is 43% higher than that of M20W045 due to a smaller quenching distance, which is discussed in Section 3.2.

3.2. Influence of wall temperature

The wall temperature of an engine cylinder has important effects on wall heat transfer. Thus, the influence of wall temperature on the wall heat flux is investigated in this section. The equivalence ratio, EGR ratio and initial pressure is fixed at 0.5, 20% and 10 atm, respectively. Both methane–air and *n*-heptane–air flames are considered since low-temperature chemistry of *n*-heptane flames will be influenced by the wall temperature. Fig. 4 shows the wall heat flux development at different wall temperature conditions. It should be noted that wall temperatures higher than 900 K was conducted for *n*-heptane flames as well, but only the results of $T_{wall} = 450 - 900$ K are shown since autoignition

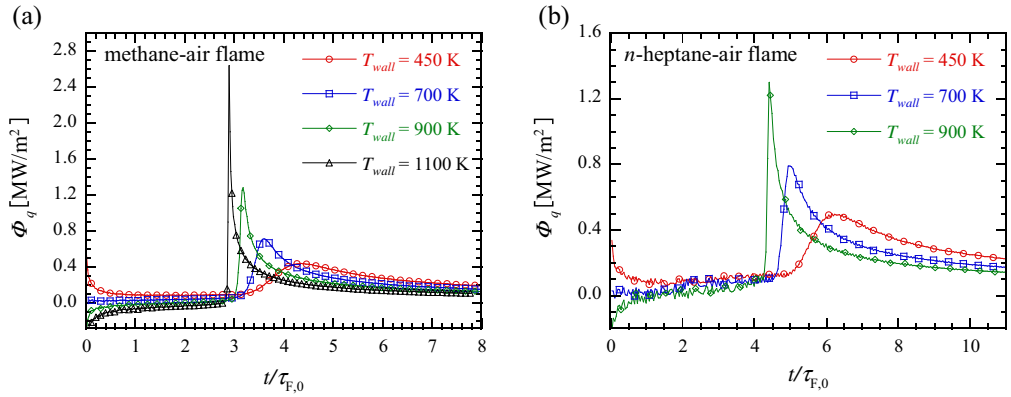

Fig. 4. Temporal developments of wall heat flux at different wall temperature conditions for methane–air (a) and *n*-heptane–air (b) flames.

occurred near the hot wall region. Wall heat flux induced by the burned gas temperature decreases slightly due to the decrease in temperature difference between the wall and burned gas, when higher wall temperatures are considered. It should be noted that insensitivity of the τ_{fw} normalized by $\tau_{F,0}$, which is explained in Section 3.1, still holds for *n*-heptane flame at $T_{wall} = 450$ K and has a value of $0.77\tau_{F,0}$. Thus, this insensitivity is not influenced by the presence of two-stage ignition of large hydrocarbon flames.

The maximum Φ_q increases drastically with increasing wall temperature, and the maximum Φ_q of *n*-heptane flames is comparable with those of methane flames. One of the contributions to this high wall heat flux can be explained by thermal conductivity of the gaseous mixture. Fig. 5 shows the maximum Φ_q and thermal conductivity of the gaseous mixture on the wall as a function of wall temperature. Clearly, the maximum Φ_q has a positive correlation with λ, suggesting that the effects of λ should be taken into account for prediction of heat loss through the wall. Another contribution can be explained by the near wall flame behavior. For higher T_{wall} cases, the unburned temperature of the reactant near the wall region increases due to heat transfer from the wall, resulting in higher flame speed and shorter quenching distance near the wall than that in the cold wall case. This phenomenon can be seen in Fig. 6, which shows the temporal development of temperature profiles with respect to wall distance for methane and *n*-heptane flames. For the methane flame at $T_{wall} = 450$ K (M20W045), the flame speed decreases steadily as it propagates, then decreases drastically in the near wall region. For $T_{wall} = 900$ K (M20W090), the flame propagation speed in the near wall region is comparable to the speed away from the wall and the flame can approach the

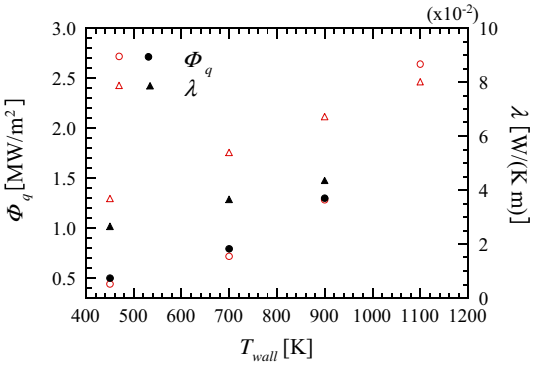

Fig. 5. Maximum wall heat flux and thermal conductivity of methane (red open symbols) and *n*-heptane (black closed symbols) as a function of wall temperature. (For interpretation of the references to color in this figure legend, the reader is referred to the web version of this article.)

wall closer than it does in the cold wall case, thereby increasing the temperature gradient near the wall. Since heat loss is lower before flame impingement occurs for hot wall cases, the maximum pressure for the hot wall cases are higher than those for cold wall cases. This also leads to a relatively thinner flame when it impinges on the wall. This trend is observed for both fuels (see Fig. 6c and d).

Low temperature heat release (LTHR), which is observed for large hydrocarbon flames under high pressure conditions, occurs between the wall and the flame front which is the location of the maximum heat release rate. Although this increases the unburned temperature by approximately 100 K, which can be seen in Fig. 6c and d, it does not seem to have significant effects on the wall heat flux induced by temperature differences between the preheated temperature of the fuel mixture and the wall as shown in Fig. 4b. The peak and burned-gas-induced heat flux still seem to be dominant. Note that according to the study by Popp et al. [6], including the Soret effect or surface reaction at wall temperatures larger than 400 K affects the maximum wall heat flux, and decreases the discrepancies between experimental and numerical results. However, in their results, although the maximum value of wall heat flux is overestimated by about 10–20% without the Soret effect or surface reaction, the general trend of wall heat flux with wall temperature is not influenced. Therefore, exclusion of the Soret effect and surface reaction does not unduly change the conclusion of the present study.

The wall temperature seems to significantly affect the quenching distance. Fig. 7 shows the temporal developments of distance between wall and flames for cases of P_{ini} = 10 atm (M20W045) and P_{ini} = 20 atm (M20W045P). The wall temperature, EGR ratio and equivalence ratio are fixed at 450 K, 20% and 0.5, respectively to see the effects of chamber pressure on the quenching distance. Here, the flame position is identified as the location of the maximum heat release rate. The minimum value indicates the quenching distance, q_d, which decreases from 0.17 mm to 0.11 mm when the pressure is doubled. As shown in Fig. 7, this quenching distance may be measurable in scalar measurements since the trend is fully reproducible by using $[CH_2O] \times [OH]$ product [24,25]. The quenching distances and peak Φ_q of all cases are summarized in Table 2. It can be seen that the wall temperature has a higher impact on the quenching distance than pressure change in the domain and clearly the peak Φ_q is dependent on the quenching distance.

The maximum Φ_q for all cases are normalized using the laminar flame power ($\Phi_f = \rho_{u,0} c_{p,u,0} (T_b - T_u) S_{L,0}$) obtained from the initial flame conditions, where ρ and c_p denote the density and specific heat at constant pressure, respectively. The subscript u and b indicate the unburned and burned sides, respectively. The normalized maximum wall heat flux, ($\Phi_n = \Phi_{q,max}/\Phi_f$), are shown in Table 2. Normalization by Φ_f, is used in many previous studies under con-

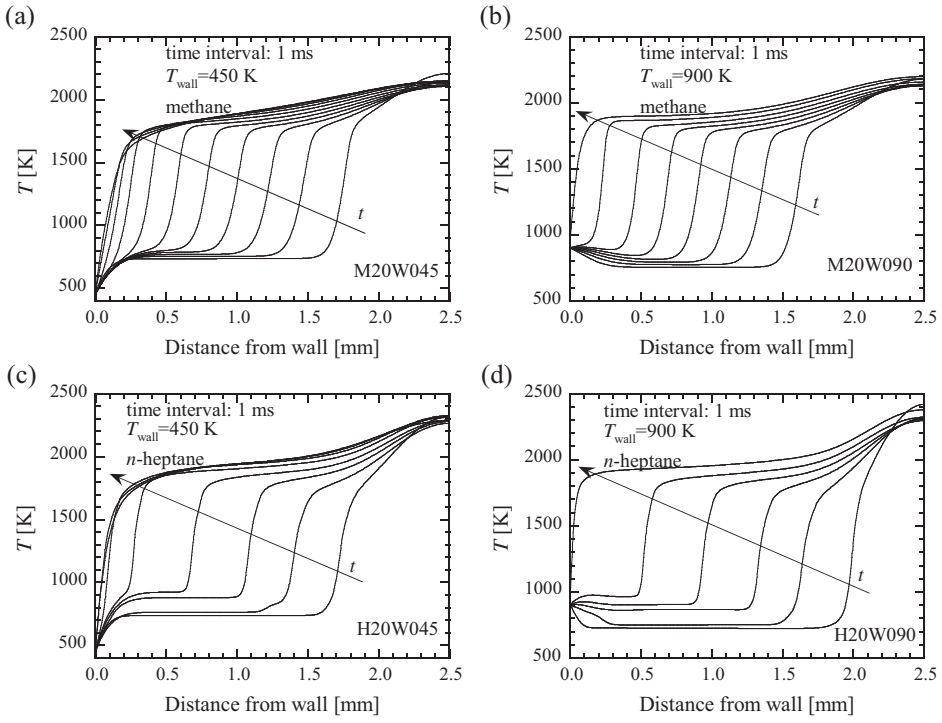

Fig. 6. Temporal developments of temperature for methane–air and *n*-heptane–air flames at different wall temperature conditions. (a, b): methane–air flames. (c, d): *n*-heptane–air flames.

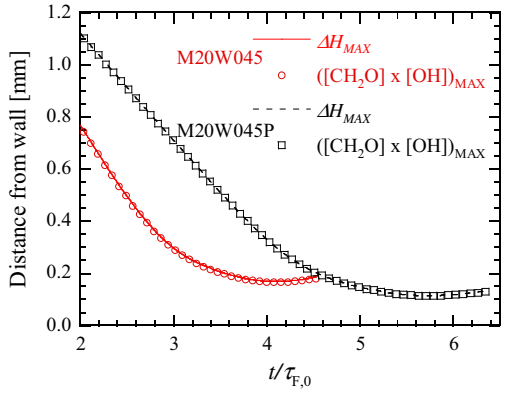

Fig. 7. Distance from wall for methane flames.

Table 2
Quenching distance, $\Phi_{q,max}$ and Φ_n.

	q_d (mm)	$\Phi_{q,max}$ (MW/m^2)	Φ_n
M10W045	0.130	0.601	0.741
M15W045	0.148	0.517	0.754
M20W045	0.169	0.438	0.770
M20W045E	0.106	0.801	0.754
M20W070	0.101	0.713	1.254
M20W090	0.059	1.283	2.255
M20W110	0.026	2.641	4.644
M20W045P	0.114	0.625	0.747
H20W045	0.071	0.497	0.535
H20W070	0.038	0.789	0.849
H20W090	0.022	1.296	1.394

stant pressure conditions [5–8,26,27]. Popp et al. [6] showed that the maximum Φ_n for a stoichiometric methane flame at atmospheric pressure is about 0.75 for chemically inactive wall boundaries and no Soret effect. This value is very close to the present methane flames at a wall temperature of 450 K, under different pressures, equivalence ratios and EGR ratios (M20W045P, M20W045, M20W045E, M10W045 & M15W045). In Table 2, the normalized maximum wall heat flux decreases with increasing mean pressure (M20W045 & M20W045P) and equivalence ratio (M20W045 & M20W045E), while Φ_n increases with an increase of wall temperature. Similar trends have been reported in previous studies for non-EGR and constant pressure cases [5–8,23,26,27], and clearly the present results show that this can be extended to isochoric and diluted conditions. This, together with the flame marker (pixel by pixel multiplication of mole fractions of CH_2O and OH) shown in Fig. 7, can be used in experimental studies to further our understanding of underlying physics of wall heat loss.

4. Conclusions

In this study, one-dimensional DNS of lean methane–air and *n*-heptane–air premixed flames with high EGR ratios propagating towards isothermal and inert walls in a head-on quenching configuration are conducted under an isochoric process to investigate wall heat flux and quenching distance at elevated pressure conditions. The effects of EGR ratio, equivalence ratio, initial pressure and wall temperature on flame–wall interaction are examined.

Increased EGR ratios result in reduced maximum wall heat flux and burned-gas-induced wall heat flux. It was found that changes in the equivalence ratio of the fuel mixture have a higher impact on the maximum wall heat flux than changes in the EGR ratio. Thus, leaner and more diluted combustion conditions are desirable on the heat loss point of view. The flame–wall interaction time, $\tau_{fw}/\tau_{F,0}$, is not influenced by changing the EGR ratio, equivalence ratio and initial chamber pressure for methane–air and *n*-heptane–air flames at fixed wall temperature conditions. The dimensional flame–wall interaction time is almost constant when the chamber pressure is doubled. The influence of the low temper-

ature oxidation in *n*-heptane flames on wall heat flux induced by temperature differences between the preheated temperature of the fuel mixture and the wall was found to be insignificant. It was also shown that the thermal conductivity near the wall, as well as the quenching distance, are sensitive to the wall temperature, and have a substantial influence on the wall heat flux.

The present results also show that the findings in previous studies [5–8,23,26,27] can be applied in a straightforward manner even for heat loss phenomenon under pressure-varying conditions with/without low-temperature chemistry in a range of ϕ, γ, P_{ini} and T_{wall}. Effects of turbulent motion on heat loss characteristics will be investigated in future research.

Acknowledgments

This work was partly supported by Council for Science, Technology and Innovation (CSTI), Cross-ministerial Strategic Innovation Promotion Program (SIP), Innovative Combustion Technology (Funding agency: JST).

References

[1] Ratnak S, Kusaka J, Daisho Y, Yoshimura K, Nakama K. Thermal efficiency improvement of a lean-boosted spark ignition engine by multidimensional simulation with detailed chemical kinetics. Int J Automotive Eng 2015;6:97–104.
[2] Hoepke B, Jannsen S, Kasseris E, Cheng W. EGR effects on boosted SI engine operation and knock integral correlation. SAE Int J Engines 2012;5:547–59.
[3] Dabireau F, Cuenot B, Vermorel O, Poinsot T. Interaction of flames of $H_2 + O_2$ with inert walls. Combust Flame 2003;135:123–33.
[4] Owston R, Magi V, Abraham J. Interactions of hydrogen flames with walls: influence of wall temperature, pressure, equivalence ratio, and diluents. Int J Hydrogen Energy 2007;32:2094–104.
[5] Owston R, Magi V, Abraham J. A numerical study of thermal and chemical effects in interactions of n-heptane flames with a single surface. Combust Flame 2007;148:127–47.
[6] Popp P, Smooke M, Baum M. Heterogeneous/homogeneous reaction and transport coupling during flame-wall interaction. Symp (Int) Combust 1996;26:2693–700.
[7] Popp P, Baum M. Analysis of wall heat fluxes, reaction mechanisms, and unburnt hydrocarbons during the head-on quenching of a laminar methane flame. Combust Flame 1997;108:327–48.
[8] Hasse C, Bollig M, Peters N, Dwyer H. Quenching of laminar iso-octane flames at cold walls. Combust Flame 2000;122:117–29.
[9] Ezekoye O, Greif R, Sawyer R. Increased surface temperature effects on wall heat transfer during unsteady flame quenching. Symp (Int) Combust 1992;24:1465–72.
[10] Connelly L, Greif R, Sawyer R, Lee D. Increased surface temperature effects on wall heat transfer during unsteady flame quenching. The Combustion Institute/Western State Section, Berkeley. Paper no. 92 – 109; 1992.
[11] Dreizler A, Böhm B. Advanced laser diagnostics for an improved understanding of premixed flame-wall interactions. Proc Combust Inst 2015;35:37–64.
[12] Yenerdag B, Fukushima N, Shimura M, Tanahashi M, Miyauchi T. Turbulence-flame interaction and fractal characteristics of H_2-air premixed flame under pressure rising condition. Proc Combust Inst 2015;35:1277–85.
[13] Yenerdag B, Minamoto Y, Naka Y, Shimura M, Tanahashi M. Flame propagation and heat transfer characteristics of a hydrogen-air premixed flame in a constant volume vessel. Int J Hydrogen Energy 2016;41:9679–89.
[14] Tanahashi M, Fujimura M, Miyauchi T. Coherent fine-scale eddies in turbulent premixed flames. Proc Combust Inst 2000;28:529–35.
[15] Smith G, Golden D, Frenklach M, Moriarty N, Eiteneer B, Goldenberg M, et al. GRI-Mech 3.0; 1999. <http://www.me.berkeley.edu/gri_mech/>.
[16] Maroteaux F, Noel L. Development of a reduced n-heptane oxidation mechanism for HCCI combustion modeling. Combust Flame 2006;146:246–67.
[17] Kee RJ, Dixon-Lewis G, Warnatz J, Coltrin ME, Miller JA. A fortran computer code package for the evaluation of gas-phase multicomponent transport properties. Sandia National Laboratories: report no. SAND86-8246; 1986.
[18] Kee RJ, Rupley FM, Miller JA. A fortran chemical kinetics package for the analysis of gas phase chemical kinetics. Sandia National Laboratories: report no. SAND89-8009B; 1989.
[19] Lele SK. Compact finite difference schemes with spectral-like resolution. J Comput Phys 1992;103:16–42.
[20] Brown P, Byrne G, Hindmarsh A. VODE: a variable-coefficient ode solver. SIAM J Sci Stat Comput 1989;10:1038–51.
[21] Baum M, Poinsot T, Thevenin D. Accurate boundary conditions for multicomponent reactive flows. J Comput Phys 1995;116:247–61.
[22] Poinsot T, Lele S. Boundary conditions for direct simulations of compressible viscous flows. J Comput Phys 1992;101:104–29.
[23] Sotton J, Boust B, Labuda SA, Bellenoue M. Head-on quenching of transient laminar flame: heat flux and quenching distance measurements. Combust Sci Technol 2005;177:1305–22.
[24] Najm HN, Paul PH, Mueller CJ, Wyckoff PS. On the adequacy of certain experimental observables as measurements of flame burning rate. Combust Flame 1998;113:312–32.
[25] Paul PH, Najm HN. Planar laser-induced fluorescence imaging of flame heat release rate. Symp (Int) Combust 1998;27:43–50.
[26] Huang W, Vosen S, Greif R. Heat transfer during laminar flame quenching: effect of fuels. Symp (Int) Combust 1988;21:1853–60.
[27] Vosen S, Greif R, Westbrook C. Unsteady heat transfer during laminar flame quenching. Symp (Int) Combust 1985;20:75–83.